

1 Laboratory studies of the aqueous-phase oxidation of 2 polyols: Submicron particles vs. bulk aqueous solution

3

4 **K. E. Daumit, A. J. Carrasquillo, J. F. Hunter, J. H. Kroll**

5 Department of Civil and Environmental Engineering, Massachusetts Institute of Technology,
6 Cambridge, MA 02139, USA

7 Correspondence to: J. H. Kroll (jhkroll@mit.edu)

8

9 **Abstract**

10 Oxidation in the atmospheric aqueous phase (cloud droplets and deliquesced particles) has
11 received recent attention as a potential pathway for the formation of highly oxidized organic
12 aerosol. Most laboratory studies of aqueous-phase oxidation, however, are carried out in bulk
13 solutions rather than aqueous droplets. Here we describe experiments in which aqueous oxidation
14 of polyols (water-soluble species with chemical formula $C_nH_{2n+2}O_n$) is carried out within
15 submicron particles in an environmental chamber, allowing for significant gas-particle
16 partitioning of reactants, intermediates, and products. Dark Fenton chemistry is used as a source
17 of hydroxyl radicals, and oxidation is monitored using a high-resolution aerosol mass
18 spectrometer (AMS). Aqueous oxidation is rapid, and results in the formation of particulate
19 oxalate; this is accompanied by substantial loss of carbon to the gas phase, indicating the
20 formation of volatile products. Results are compared to those from analogous oxidation reactions
21 carried out in bulk solution. The bulk-phase chemistry is similar to that in the particles, but with
22 substantially less carbon loss. This is likely due to differences in partitioning of early-generation
23 products, which evaporate out of the aqueous phase under chamber conditions (in which liquid
24 water content is low), but remain in solution for further aqueous processing in the bulk phase.
25 This work suggests that the product distributions from oxidation in aqueous aerosol may be
26 substantially different from those in bulk oxidation experiments. This highlights the need for
27 aqueous oxidation studies to be carried out under atmospherically relevant partitioning conditions,
28 with liquid water contents mimicking those of cloud droplets or aqueous aerosol.

1 **1 Introduction**

2 A large fraction of atmospheric organic aerosol (OA) is known to be secondary in nature, formed
3 by the oxidation and subsequent condensation of gas-phase precursors. However, the sources and
4 formation mechanisms for the most oxidized fraction of OA remain highly uncertain. Ambient
5 measurements indicate that the most highly oxidized OA has an average carbon oxidation state of
6 between 0 and +1 (Daumit et al., 2013; Jimenez et al., 2009; Kroll et al., 2011) and can form
7 rapidly over short time scales (approximately 1 to 3 days (Jimenez et al., 2009; Volkamer et al.,
8 2006)). However, the organic aerosol formed in laboratory studies is typically substantially less
9 oxidized than this (Donahue et al., 2012; Heald et al., 2010; Kroll et al., 2011; Qi et al., 2010),
10 and model studies generally have difficulty reproducing the same level of oxidation in such short
11 time scales (Dzepina et al., 2009; 2011; Hodzic et al., 2010; Lee-Taylor et al., 2011).

12 Aqueous-phase oxidation has received considerable attention as a potential formation pathway for
13 highly oxidized organic aerosol (Ervens et al., 2011; Lim et al., 2010). The oxidation of organic
14 species in the aqueous phase has recently been investigated in the laboratory for a range of water-
15 soluble species, including small carbonyls (Altieri et al., 2008; Carlton et al., 2007; Kirkland et al.,
16 2013; Perri et al., 2009; 2010; Tan et al., 2009; 2010), isoprene and its oxidation products (Altieri
17 et al., 2006; Kameel et al., 2013; Liu et al., 2012a; Renard et al., 2013; Zhang et al., 2010), and
18 phenolic compounds (Smith et al., 2014; Sun et al., 2010). Such bulk-phase studies have clearly
19 demonstrated that aqueous-phase oxidation, when it occurs, can lead to the rapid formation of
20 highly oxidized organic species.

21 The importance of such oxidation processes relies critically on partitioning (Donahue et al.,
22 2014): a compound will undergo aqueous-phase oxidation only if it is primarily partitioned to the
23 atmospheric aqueous phase (cloud droplets or aqueous submicron particles), rather than the gas or
24 condensed-organic phase. The partitioning between the gas and aqueous phases is determined by
25 a compound's effective Henry's Law constant (H^*) (or alternatively its saturation vapor
26 concentration over water (c_{aq}^*) (Ervens et al., 2011)), as well the liquid water content (LWC) of
27 the air mass, as shown in Eq. 1:

$$28 \quad f_{aq} = \frac{(LWC)H^*RT}{10^{12} + (LWC)H^*RT} = \frac{LWC/c_{aq}^*}{1 + LWC/c_{aq}^*} \quad (1)$$

29 in which f_{aq} is the equilibrium fraction in the aqueous phase, LWC is in units of $\mu\text{g m}^{-3}$, H^* is in

1 units of M atm^{-1} , and c_{aq}^* is in units of $\mu\text{g m}^{-3}$ and is equal to $10^{12} H^* R^{-1} T^{-1}$ (where $R = 0.0821$
2 $\text{L atm mol}^{-1} \text{K}^{-1}$ and T is temperature in K). By Eq. 1, the partitioning of a single compound (with
3 a fixed H^* or c_{aq}^*) can be very different for different values of LWC. Atmospheric LWCs can
4 span many orders of magnitude, ranging from ~ 1 to $100 \mu\text{g m}^{-3}$ for aqueous aerosol, and $\sim 10^5$ to
5 $10^6 \mu\text{g m}^{-3}$ for cloud droplets (Ervens et al., 2011), while a bulk aqueous solution has a LWC on
6 the order of $10^{12} \mu\text{g m}^{-3}$ (the density of water). Therefore, f_{aq} for a given compound will also vary
7 by many orders of magnitude for these systems, as illustrated in Figure 1. Many compounds that
8 are considered to be “water-soluble” for bulk solutions (H^* of 1-1000 M atm^{-1}) will not actually
9 partition significantly into aqueous submicron particles, or even into cloud droplets. This could
10 have an important influence on the resulting chemistry, and suggests that a bulk solution may not
11 always accurately represent aqueous processing under atmospheric conditions.

12 Some recent bulk-solution experiments have begun to examine the role of gas-particle
13 partitioning under lower-LWC conditions, by atomizing or nebulizing the bulk aqueous solution
14 as it undergoes aqueous oxidation (Lee et al., 2011a; 2011b; 2012; Liu et al., 2012b; Ortiz-
15 Montalvo et al., 2012; Zhao et al., 2012). While these studies do indeed show loss of the most
16 volatile species formed, leaving behind only low-volatility condensed-phase products, the
17 chemistry that forms these products still takes place in the bulk aqueous solution, with limited
18 partitioning into the gas phase. To our knowledge, only two studies (Nguyen et al., 2013;
19 Volkamer et al., 2009) have examined oxidation chemistry within aqueous droplets themselves,
20 allowing for gas-particle partitioning that mimics what may occur in the atmosphere. These
21 studies found enhanced uptake and aerosol yield from glyoxal (Volkamer et al., 2009) and
22 glycolaldehyde (Nguyen et al., 2013) in the presence of aqueous submicron particles; results from
23 these experiments have not been explicitly compared to those in which oxidation was carried out
24 in bulk solutions.

25 Here we describe laboratory studies of the oxidation of water-soluble organic species in the
26 aqueous phase, with experiments conducted both within bulk aqueous solutions and within
27 submicron aqueous particles. The goal of these experiments is to compare the oxidation
28 chemistry under very different partitioning conditions. We focus on the oxidation of polyols with
29 the chemical formula $\text{C}_n\text{H}_{2n+2}\text{O}_n$ (with one hydroxyl group on each carbon atom). Polyols with
30 four or more carbon atoms have exceedingly high values of H^* ($> 10^{16} \text{M atm}^{-1}$ (Sander, 1999)),

1 ensuring they will be present in the aqueous phase even at the low LWC in our chamber; thus any
2 observed partitioning will involve reaction intermediates and products only. To our knowledge,
3 this work is the first direct comparison of aqueous oxidation in submicron particles and in bulk
4 aqueous solution.

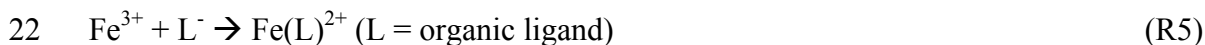
5

6 **2 Experimental Methods**

7 Two sets of experiments are conducted: (1) bulk oxidation, in which reactions take place within a
8 bulk aqueous solution of ~0.5 L volume, and (2) chamber oxidation, in which reactions take place
9 within submicron aqueous particles in an environmental chamber. Both sets of experiments use
10 dark Fenton chemistry (Fe^{2+} and hydrogen peroxide) as an aqueous-phase source of oxidants.
11 While there is some uncertainty as to the exact oxidant-forming mechanisms in Fenton systems,
12 in part due to the complex iron speciation, it is likely that hydroxyl radicals (OH) are the
13 predominant oxidant formed in our experiments (Ma et al., 2006; Southworth and Voelker, 2003).
14 Fe^{2+} reacts with hydrogen peroxide (H_2O_2) to produce OH and Fe^{3+} , which is subsequently
15 converted back to Fe^{2+} via reaction with other species:



19 Alternatively, Fe^{3+} can form complexes with water or organic acids; these pathways compete
20 with the regeneration of Fe^{2+} and can eventually slow the production of OH:



23 A more detailed treatment of this chemistry is described elsewhere (Arakaki and Faust, 1998;
24 Faust and Hoigne, 1990; Hoffmann et al., 1996; Ma et al., 2006; Nguyen et al., 2013; Ou et al.,
25 2008). In both sets of experiments, we start with a mixture of a polyol and Fe^{2+} , and initiate the
26 oxidation chemistry with the addition of H_2O_2 . The use of Fenton chemistry to initiate oxidation
27 within aqueous submicron particles was first demonstrated in a recent glycolaldehyde uptake
28 study by Nguyen et al. (2013); the present experiments differ from that work in that we focus on

1 dark Fenton chemistry, using the addition of H₂O₂ rather than exposure to UV lights to initiate
2 the reaction.

3

4 **2.1 Bulk aqueous oxidation**

5 For bulk oxidation experiments, the general technique of Lee et al. (2011a) is used, in which an
6 atomizer serves both as the reactor containing the aqueous solution and as the method for
7 aerosolizing the solution, enabling online analysis by aerosol instrumentation. Figure 2a shows a
8 simple schematic of the experimental setup. Reactions are carried out in a 1 L borosilicate
9 reaction bottle, and the solution is continuously atomized using a constant output atomizer (TSI,
10 Model 3076) with a backing pressure of ~30 psi of pure compressed air (Aadco 737-13A/C with
11 methane reactor), giving 2.5-3 LPM aerosol output flow. The atomizer output is passed through
12 an empty 1 L bottle to remove excess liquid water, then through a diffusion dryer, and finally into
13 the aerosol instruments, described in Section 2.3.

14 A major difference between the present experiments and previous bulk oxidation experiments
15 (Lee et al., 2011a; 2011b; 2012; Liu et al., 2012b; Ortiz-Montalvo et al., 2012; Zhao et al., 2012)
16 is the oxidation scheme: here OH radicals are generated via dark Fenton chemistry rather than
17 photolysis of hydrogen peroxide, avoiding the use of 254 nm lights. The initial atomization
18 solution contains iron(II) sulfate heptahydrate (99+%) and a polyol (glycerol, 99.5+%, erythritol,
19 99+%, adonitol 99+%, mannitol 98+%, or volemitol, all Sigma-Aldrich) fully dissolved in Milli-
20 Q water; concentrations are given in Table 1. Prior to H₂O₂ addition, this solution is atomized
21 into the AMS (see below) to characterize the reactants and ensure they are inert with respect to
22 each other. To initiate Fenton chemistry, hydrogen peroxide (30% w/w in water, Alfa Aesar) is
23 added and the solution is shaken to facilitate mixing. After ~3 hours, once the reaction appears to
24 have gone to completion, the solution is exposed to UV light for additional oxidation (via photo-
25 Fenton chemistry) and/or direct photolysis, using four external blacklights (Sylvania BL-350
26 ECO, output 300-400 nm). Photo-Fenton reactions regenerate Fe²⁺ and can produce additional
27 OH:



1 **2.2 Chamber oxidation**

2 Chamber experiments are conducted to allow for aqueous oxidation in submicron particles,
3 providing partitioning conditions representative of deliquesced atmospheric aerosol. The chamber
4 oxidation setup is shown in Figure 2b. The MIT chamber is a 7.5 m³ Teflon (5 mil PFA) bag
5 within a temperature-controlled environmental room. Two banks of 24 blacklights (Sylvania BL-
6 350 ECO) on opposite sides of the chamber provide UV irradiation when needed. The chamber is
7 run as a semi-batch reactor with 5 LPM pure air added to balance instrument sample flows. A
8 fraction of this air is sent through a bubbler containing Milli-Q water in order to maintain a
9 relative humidity of between 67% and 79%, ensuring that all sulfate-containing particles are
10 aqueous. Prior to reaction, seed particles composed of iron(II) sulfate (FeSO₄) and a polyol are
11 introduced into the chamber via atomization. The liquid water content in the chamber is not
12 directly measured, but is estimated to be in the range of ~20 to ~150 μg m⁻³ prior to oxidation,
13 based on concentrations of particulate water measured by the AMS. These values are broadly
14 consistent with liquid water contents estimated by assuming the particles have a similar
15 hygroscopic growth factor as particles of ammonium sulfate (Seinfeld & Pandis, 2006).
16 Concentrations of the atomizer solution are given in Table 1; it should be noted that within the
17 aqueous particles themselves, concentrations will be substantially higher than these values, since
18 the solution is concentrated upon atomization by a factor of ~1000 (based on measured mass
19 loadings and estimated LWC).

20 Seed particles are allowed to mix in the chamber for one hour prior to addition of H₂O₂, which
21 initiates the reaction. H₂O₂ is not added directly to the atomizer solution since this would initiate
22 oxidation in the bulk solution prior to atomization, and so is instead introduced in the gas phase,
23 from which it subsequently partitions into the aqueous phase. Gas-phase H₂O₂ is introduced by
24 sending 1-1.5 LPM air through a two-neck flask containing 6.0 μL of 30% aqueous H₂O₂ solution
25 and into the chamber via a Teflon line; full evaporation of the H₂O₂ takes approximately 30 min.
26 Assuming all the H₂O₂ enters the chamber, and partitions into the aqueous particles according to
27 Henry's law (with $H^* = 10^5 \text{ M atm}^{-1}$ (Sander, 1999)), this gives 270 ppb H₂O₂ in the gas phase,
28 and 27 mM in the aqueous particles. This aqueous concentration is higher than in the bulk
29 experiments, but the concentrations of Fe²⁺ and polyol are also higher in the particles than in the
30 bulk solution. However, because some H₂O₂ is expected to be lost to surfaces, such as the Teflon

1 inlet tubing and chamber walls, these H₂O₂ concentrations likely represent upper limits. After
2 completion of the dark Fenton chemistry, the blacklights are turned on for additional photolytic
3 and/or oxidative chemistry, as in the bulk experiments. Under dark conditions, gas-phase
4 oxidation is unlikely; however, during irradiation the photolysis of H₂O₂ will lead to the
5 formation of some gas-phase OH; as discussed below, this is unlikely to affect the observed
6 chemistry.

7

8 **2.3 Aerosol analysis**

9 Aerosol size distribution, volume, and number density are monitored using a scanning mobility
10 particle sizer (SMPS, TSI, Inc.). Chemical composition of non-refractory particulate matter is
11 measured using a high-resolution time-of-flight aerosol mass spectrometer (AMS, Aerodyne
12 Research, Inc.). This allows for the measurement of chemical families, such as total organic,
13 sulfate, and ammonium (Canagaratna et al., 2007; DeCarlo et al., 2006), as well as elemental
14 ratios of the organic species, most importantly oxygen-to-carbon (O/C) and hydrogen-to-carbon
15 (H/C) (Aiken et al., 2007; 2008). All data reported here was taken with the instrument operated in
16 V mode. Because the amount of sulfate per particle is constant, abundances of all reported ions
17 and families are normalized to sulfate, accounting for possible changes in collection efficiency
18 (CE), variations in atomizer output, dilution in the chamber or atomizer, and loss of particles to
19 surfaces. Some sulfate signal (10-25%) is measured in the “closed” mass spectra, suggesting that
20 FeSO₄ does not flash-vaporize at the temperature of the AMS vaporizer (~550-600°C). However,
21 this fraction does not vary significantly over any experiment, suggesting the AMS “diff” signal is
22 sufficient for this normalization. In most chamber experiments the aerosol is not sent through a
23 dryer prior to analysis, though drying appears to have no effect on measured elemental ratios or
24 sulfate-normalized concentrations. For chamber oxidation experiments, we also monitor
25 temperature and relative humidity (Vaisala), NO_x (Horiba, Inc.), and ozone (2B Tech).

26

27 **3 Results and Discussion**

28 A series of control experiments were carried out to verify that aqueous-phase, dark Fenton
29 chemistry was indeed responsible for any chemistry observed. No reaction was observed between

1 the polyols and FeSO₄ in the absence of H₂O₂, nor between the polyols and H₂O₂ in the absence
2 of FeSO₄, confirming that both Fe²⁺ and H₂O₂ are necessary for oxidation to occur. Furthermore,
3 no chemical changes were observed upon addition of H₂O₂ or exposure to UV when a chamber
4 experiment (using erythritol-FeSO₄ particles) was conducted under dry conditions (RH < 4%).
5 The sulfate-normalized organic signal gradually decayed over the course of this experiment, but
6 this is likely a result of gradual evaporation of organic material as the chamber air is diluted. The
7 lack of a reaction under such dry conditions confirms that the chemistry described below indeed
8 takes place only in the aqueous phase.

9

10 **3.1 Bulk oxidation of erythritol**

11 Results for the bulk oxidation of erythritol (C₄H₁₀O₄) are shown in Fig. 3. Figure 3a shows the
12 aerosol mass spectrum of the aqueous erythritol solution, taken over a 30-minute period
13 immediately prior to the addition of H₂O₂. Figure 3b shows the time traces of key AMS ions and
14 species (all normalized to sulfate). Once H₂O₂ is added, oxidation occurs immediately. Key ions
15 associated with erythritol (*m/z* 29, 39, 61, 73, 91) begin to decay rapidly, presumably by reaction
16 with OH. Using a *k*_{OH} of 1.9 x 10⁹ M⁻¹ s⁻¹ (Herrmann et al., 2010), this decay is consistent with an
17 initial aqueous OH concentration of 4.8 x 10⁻¹² M, which is within an order of magnitude of the
18 average OH concentrations estimated for ambient deliquesced particles (Herrmann et al., 2010).
19 The OH concentration, estimated from the time dependence of the polyol concentration (see
20 Supporting Information), drops over the course of the experiment, reaching a final OH exposure
21 of 2.7 x 10⁻⁹ M s. Sulfate-normalized organic signal initially decreases, likely due to the
22 formation and evaporation of compounds that are more volatile than erythritol, but then gradually
23 rises, presumably from the addition of oxygen-containing functional groups that increase the
24 molecular weight and reduce the volatility of the organic species. Ammonium (NH₄⁺) also rises,
25 likely due to uptake of ammonia from the laboratory air; this is consistent with acidification of
26 the solution, which is known to occur upon initiation of dark Fenton chemistry (Nguyen et al.,
27 2013). This is accompanied by an instantaneous change in the appearance of the atomizer
28 solution from colorless to yellow-orange, consistent with the formation of Fe(OH)²⁺ (Zuo and
29 Hoigne, 1992).

1 Rapid growth of the CO_2^+ ion in the AMS is observed upon oxidation (Fig. 3b). This highly
2 oxidized ion fragment, which typically indicates the presence of carboxylic acids, is the most
3 abundant ion in the product mass spectra, shown in Fig. 3c. Figure 3d shows the elemental ratios
4 of the particulate organic species as a function of time; the rapid rise in O/C and drop in H/C
5 upon addition of H_2O_2 is also consistent with rapid oxidation of the organic species. It should be
6 noted that the initial H/C and O/C measured by the AMS do not match the true values for
7 erythritol. This is a result of using the default elemental analysis correction factors, which have
8 been determined empirically for an ensemble of species rather than individual compounds (Aiken
9 et al., 2008); however, errors in the absolute elemental ratios are not expected to affect the
10 observed trends in H/C and O/C, nor the overall conclusions of this work. The rapid oxidation of
11 dissolved organic species observed here is broadly consistent with the findings of other bulk
12 oxidation studies (Altieri et al., 2006; 2008; Carlton et al., 2007; Kirkland et al., 2013; Lee et al.,
13 2011a; 2011b; 2012; Liu et al., 2012a; Perri et al., 2009; Sun et al., 2010; Tan et al., 2009; 2010;
14 Zhang et al., 2010; Zhao et al., 2012).

15 The AMS mass spectrum of the oxidation products closely resembles that of oxalate ($\text{C}_2\text{O}_4^{2-}$)
16 (Mensah et al., 2011; Takegawa et al., 2007), which has been shown to be a major product in
17 other aqueous-phase oxidation systems (Carlton et al., 2007; Perri et al., 2009; Tan et al., 2010).
18 A pathway for the formation of oxalic acid from the aqueous oxidation of ethylene glycol (a C2
19 diol) has been shown by Tilgner & Herrmann (2010) and mechanisms for the formation of oxalic
20 acid from larger diacids have been described by Ervens et al. (2004). We did not observe the
21 formation of organonitrogen compounds, which were major reaction products in the uptake of
22 glyoxal (Galloway et al., 2009; Nozière et al., 2009) and glycolaldehyde (Nguyen et al., 2013). In
23 those studies, imidazoles and other N-containing products were formed via nucleophilic attack of
24 ketones and aldehydes by ammonia (Galloway et al., 2009; Nozière et al., 2009); such reactions
25 are unlikely in the present system given the lack of carbonyl moieties in the polyols studied here.

26 The formation of oxalate (a highly-oxidized C2 compound) from erythritol (a less-oxidized C4
27 compound) likely occurs via multiple generations of oxidation. Individual product ions (not
28 shown) have significantly different temporal behavior, with some growing in and decaying before
29 others, suggesting complex chemistry with intermediate products formed at different stages of

1 oxidation. The varying rates of decay of erythritol ions in Fig. 3b (e.g., m/z 61 vs. 91) provide
2 further evidence that multigenerational oxidation is occurring in this system.

3 Upon exposure to UV, the organic ions decay still further, and the total organic signal decreases
4 dramatically, in a short period of time (lifetime ~ 36 min; see Fig. S1a, Supporting Information).
5 This is likely a result of either further oxidation by OH generated from photo-Fenton chemistry
6 (R6) or direct photolysis (R7) to form small volatile species that cannot be detected by the AMS.
7 This provides additional evidence for oxalate, since Fe(III) oxalato complexes are known to
8 rapidly photolyze, a process that has been suggested as an important sink of atmospheric oxalate
9 (Sorooshian et al., 2013). Given the abundance of iron in the system, our results suggest that the
10 main condensed-phase oxidation product is oxalate, present as an iron oxalato complex.

11

12 **3.2 Chamber oxidation of erythritol**

13 Results for the oxidation of erythritol in aqueous particles in the chamber are shown in Fig. 4. As
14 in the bulk experiment, dark Fenton chemistry within submicron particles in the chamber was
15 found to lead to the rapid decay of erythritol and formation of oxidized products. A maximum
16 OH concentration of 3.5×10^{-12} M is reached between 30 and 40 min, and subsequently decreases
17 to give a final OH exposure of 4×10^9 M s; these values are similar (within a factor of two) to
18 those of the bulk experiments. The initial organic mass spectrum of unreacted erythritol in the
19 chamber (Fig. 4a) closely matches that of erythritol in the bulk (Fig. 3a). The observed chemical
20 changes in the two oxidation systems, as described by the time traces of key AMS ions from the
21 chamber experiment (Fig. 4b), the product mass spectrum (Fig. 4c), and changes to O/C and H/C
22 (Fig. 4d) are also similar to the bulk oxidation results. The primary difference is that the total
23 organic signal decreases substantially more than in the bulk, with no subsequent increase,
24 discussed in detail below. As in the bulk experiment, a rapid loss of organic mass is observed
25 upon UV irradiation (Fig. S1b). This loss is unlikely to arise from oxidation by gas-phase OH
26 (formed from H_2O_2 photolysis): the rapid loss of the organic species (lifetime ~ 7 min) would
27 require an OH mixing ratio of $> 6 \times 10^7$ molec cm^{-3} (assuming a k_{OH} of $< 3 \times 10^{-11}$ $\text{cm}^3 \text{ molec}^{-1} \text{ s}^{-1}$),
28 far greater than can be produced by H_2O_2 photolysis. Instead, the rapid loss of organic mass

1 probably arises from the direct photolysis of Fe(III) oxalato complexes, as in the bulk oxidation
2 experiment.

3 Our finding of rapid oxidation by Fenton chemistry in the absence of UV light differs from the
4 results of Nguyen et al. (2013), who found oxidation to occur only upon UV irradiation (photo-
5 Fenton chemistry). In that work, the H₂O₂ was added directly to the atomizer solution (along with
6 FeSO₄), and so dark Fenton chemistry may have gone to completion prior to the introduction of
7 the organic species (glycolaldehyde) in the gas phase. By contrast, in the present experiments,
8 H₂O₂ is added last, so that all OH is produced in the presence of the aerosol-phase organic
9 compound. Because of such differences, and the differences in the organic species studied, results
10 from the two chemical systems are difficult to compare directly. Nonetheless, our results are
11 broadly consistent with those of Nguyen et al., in that they indicate that aqueous-phase oxidation
12 in submicron particles can lead to the rapid formation of highly oxidized organic aerosol.

13

14 **3.3 Oxidation of other polyols**

15 Similar results are seen for the oxidation of most of the other polyols, in both the bulk phase and
16 the chamber. The one exception is the oxidation of glycerol (a C₃ polyol), which behaved
17 differently in both the bulk and chamber experiments, presumably due to its high volatility. In the
18 glycerol bulk experiments, the measured organic mass actually increased after oxidation, likely
19 because the less volatile oxidation products evaporated less than glycerol upon atomization; and
20 in the chamber experiments, the LWC was too low for any measureable particulate glycerol.
21 However, the C₅-C₇ polyols (adonitol, mannitol, and volemitol) all behaved similarly to
22 erythritol upon oxidation, with decreases in the intensity of the polyol ions and H/C, increases in
23 the CO₂⁺ ion intensity and O/C, and product mass spectra resembling that of oxalate (Figs. S2-S4
24 in the Supplement). Estimated OH concentrations and exposures were also similar between the
25 bulk and chamber cases (see Fig. S5 in the Supplement). As in the erythritol case, exposure to
26 UV led to a rapid decrease in all organic ion signal intensity, as well as a decrease in total organic
27 mass. In each case, the fraction of organic material remaining after oxidation was smaller for the
28 chamber experiment than for the bulk experiment.

1 Shown in Fig. 5 is the fraction of carbon remaining in the condensed phase (f_C) after reaction in
2 the bulk solution or deliquesced particles for each polyol (except glycerol, for which meaningful
3 values of f_C could not be determined). This is calculated from the changes in organic mass
4 concentration and elemental ratios:

$$5 \quad f_C = \frac{[\text{Org}]_f (16\text{O}/\text{C}_i + \text{H}/\text{C}_i + 12)}{[\text{Org}]_i (16\text{O}/\text{C}_f + \text{H}/\text{C}_f + 12)} \quad (2)$$

6 in which $[\text{Org}]$ is the average high-resolution sulfate-normalized mass concentration of total
7 organic, O/C and H/C are the oxygen-to-carbon and hydrogen-to-carbon ratios, respectively, of
8 the organic species, with the subscripts i and f denoting initial and final conditions (before and
9 after H_2O_2 addition), respectively. For example, in the case of erythritol oxidation, 51% of the
10 initial carbon remained after bulk oxidation, but only 16% remained after oxidation in aqueous
11 aerosol in the chamber. For all bulk experiments, between 48% and 58% of the original carbon
12 remained in the condensed phase after oxidation, with no obvious dependence on carbon number.
13 However, a clear trend is observed for the chamber experiments, with f_C increasing with the size
14 of the polyol.

15

16 **3.4 Differences between chamber and bulk experiments**

17 The above observations – that a larger fraction of carbon remains in the condensed phase for the
18 bulk experiments than for the chamber experiments, and that this difference gets smaller with
19 increasing carbon number – can be explained either by differences in reactivity or differences in
20 partitioning between the two systems. The submicron particles in the chamber have higher
21 reactant concentrations and a greater ionic strength than the dilute bulk solution, and also require
22 dissolution of gas-phase H_2O_2 prior to oxidation; these differences may cause the observed
23 differences in oxidation kinetics. Furthermore, the availability of gas-phase H_2O_2 in the chamber
24 that can partition into the submicron particles, could allow for a longer production of OH.
25 However, the ratio of polyol to Fe^{2+} is also greater in the chamber, so the OH may react away
26 more quickly. These complex effects are difficult to quantify, but could result in different
27 chemical reactions and degrees of oxidation between the two systems.

1 Nonetheless, it is unlikely that differences in reactivity are driving the differences in f_C between
2 the bulk and chamber experiments, given the similarities in mass spectra, changes to individual
3 ions, and elemental ratios in the two cases (as shown in Figures 3, 4, and S1-4). The final OH
4 exposures for the oxidation of erythritol in the bulk solution (4.7×10^{-12} M s) and in the
5 submicron particles (2.7×10^{-9} M s) agree to within a factor of two. This is true for the larger
6 polyols (C5-C7) as well (Fig. S5), suggesting that differences in oxidant availability are not likely
7 to account for the observed differences between the bulk and chamber results. Furthermore, the
8 variation in f_C for different polyols oxidized in the chamber (Figure 5) is also unlikely to result
9 from differences in chemistry, given that the oxidation conditions were the same.

10 Rather, the difference in total organic mass remaining in the condensed phase appears to be a
11 result of differences in gas-aqueous partitioning of intermediate species (early-generation
12 oxidation products). A general mechanism is illustrated in Fig. 6. The polyol is oxidized to form
13 multiple generations of products, ultimately forming oxalate (in the form of an iron (III) oxalato
14 complex). In the bulk aqueous solution, where the liquid water content is very high, the reactants,
15 intermediates, and products remain in the condensed phase. (Some of these species may
16 evaporate upon atomization and not be detected by the AMS, but they still would have been
17 present in the condensed phase during oxidation.) However, in the chamber experiments, in
18 which LWC is low, relatively volatile compounds can partition out of the condensed phase. The
19 polyols and oxalate are sufficiently water-soluble to remain in the particle phase at this low LWC,
20 suggesting that the partitioning of intermediate compounds from the aqueous phase to the gas
21 phase (red arrow in Fig. 6) accounts for the increased loss of organic material in the chamber.
22 These early-generation oxidation products are likely to be more volatile (lower H^*) than the
23 polyol precursor, due to the oxidative conversion of hydroxyl groups to carbonyl groups (Bethel
24 et al., 2003) and/or the formation of smaller molecular species via fragmentation reactions (Kroll
25 et al., 2009). Evaporation of these species may also be promoted by a decrease in particulate
26 water, which is observed upon H_2O_2 addition and likely occurs due to a change in the
27 hygroscopicity of iron salts upon initiation of Fenton chemistry. Regardless of the exact
28 mechanism, partitioning of intermediates into the gas phase will compete with further oxidation,
29 as shown in Fig. 6, resulting in lower yields of oxalate than were measured in the bulk
30 experiments. This general mechanism also explains the correlation between f_C and carbon number

1 (Fig. 5), since the size, and thus the volatility, of the intermediate compounds should be related to
2 the size of the polyol precursor.

4 **4 Conclusions and Implications**

5 To our knowledge, this work presents the first direct comparison of aqueous-phase oxidation
6 within submicron particles to that within the bulk phase. In both systems, dark Fenton chemistry
7 leads to the rapid conversion of polyol precursors to highly-oxidized organic material, a result
8 that is broadly consistent with previous aqueous-phase oxidation studies (Altieri et al., 2006;
9 2008; Carlton et al., 2007; Kirkland et al., 2013; Lee et al., 2011a; 2011b; 2012; Liu et al., 2012a;
10 Nguyen et al., 2013; Perri et al., 2009; Sun et al., 2010; Tan et al., 2009; 2010; Zhang et al., 2010;
11 Zhao et al., 2012). The primary difference between the two systems is that less carbon remains in
12 the condensed phase in the chamber experiments, with the smallest precursors having the greatest
13 differences in f_C . As shown in Fig. 1, under bulk conditions, any compound with $H^* \gtrsim 0.1 \text{ M atm}^{-1}$
14 should be present primarily in the aqueous phase. However, at the lower LWC of the chamber,
15 compounds with H^* as high as 10^9 M atm^{-1} will instead be present predominantly in the gas phase.
16 Thus, species with H^* between these limits will remain dissolved in bulk-phase water, but will
17 partition out of submicron particles into the gas phase. Our results suggest that the reaction
18 intermediates formed from the oxidation of polyols appear to have H^* in this range. Therefore, the
19 partitioning of these early-generation products from aqueous aerosol to the gas phase can explain
20 the dramatic differences in f_C observed in the bulk and chamber experiments.

21 The present results confirm those of previous studies showing that aqueous-phase oxidation is an
22 efficient pathway for the rapid formation of highly oxidized material. However, when oxidation
23 occurs within submicron particles, the fraction of carbon remaining in the condensed phase is
24 substantially smaller than in the bulk oxidation experiments, implying that the formation of
25 highly oxidized OA by aqueous chemistry may be somewhat less important than bulk-phase
26 experiments suggest. Bulk oxidation experiments may not accurately simulate the chemistry that
27 takes place in the atmospheric aqueous phase, due to large differences in LWC (and therefore
28 partitioning) between the bulk solution and atmospheric droplets or particles. This difference
29 points to the importance of running aqueous-phase oxidation experiments under atmospherically-
30 relevant partitioning conditions. This is analogous to chamber studies of secondary organic

1 aerosol (SOA) formation via partitioning into the condensed-organic phase, which to be
2 representative of atmospheric conditions must be run at low total organic mass concentrations
3 (c_{OA}) (Presto and Donahue, 2006). A major difference between such “traditional” SOA chamber
4 experiments and aqueous-phase oxidation, however, is that LWC can vary by a great deal more
5 than c_{OA} between the laboratory and atmosphere. Our results show that even bulk oxidation
6 experiments that allow for evaporation of oxidation products (Lee et al., 2011a; 2011b; 2012; Liu
7 et al., 2012b; Ortiz-Montalvo et al., 2012; Zhao et al., 2012), may not fully simulate atmospheric
8 processing, since they do not include the effects of partitioning of reaction intermediates. Further,
9 the experiments with glycerol oxidation demonstrate that in bulk-phase experiments it is possible
10 to oxidize compounds that would not actually be present in the atmospheric aqueous phase under
11 most conditions. Results from the oxidation of larger polyols indicate that differences in LWC
12 between bulk and chamber oxidation result in significant differences in partitioning, which in turn
13 can affect the chemistry. For experiments like ours with a single product, this affects only the
14 final yield. However, when multiple oxidation products are formed, with intermediates of varying
15 volatility, changing the LWC may also alter the product distributions.

16 This study underscores the need for conducting oxidation experiments at atmospherically-
17 relevant liquid water contents, and extending the existing suite of bulk experiments to additional
18 partitioning conditions. Oxidizing previously-studied compounds (small carbonyls, acids,
19 isoprene oxidation products, etc.) within aqueous submicron particles would provide valuable
20 information on the role of partitioning and LWC on the formation of highly-oxidized OA for a
21 wider range of water-soluble organic compounds. Further, the large differences in partitioning
22 between deliquesced particles and clouds (Fig. 1) suggest that a similar set of experiments is a
23 useful next step for the accurate study of atmospheric cloud processing. Oxidation experiments
24 involving actual cloud droplets, with LWCs much higher than those of aqueous particles but still
25 far lower than that of the bulk aqueous phase, would improve our understanding of this
26 potentially important source of oxidized organic aerosol.

27

28 **Acknowledgements**

29 This work was supported by the National Science Foundation, under grant number AGS-1056225.

1 **References**

- 2 Aiken, A. C., DeCarlo, P. F. and Jimenez, J. L.: Elemental analysis of organic species with
3 electron ionization high-resolution mass spectrometry, *Anal. Chem.*, 79(21), 8350–8358,
4 doi:10.1021/ac071150w, 2007.
- 5 Aiken, A. C., DeCarlo, P. F., Kroll, J. H., Worsnop, D. R., Huffman, J. A., Docherty, K. S.,
6 Ulbrich, I. M., Mohr, C., Kimmel, J. R., Sueper, D., Sun, Y., Zhang, Q., Trimborn, A., Northway,
7 M., Ziemann, P. J., Canagaratna, M. R., Onasch, T. B., Alfarra, M. R., Prevot, A. S. H., Dommen,
8 J., Duplissy, J., Metzger, A., Baltensperger, U. and Jimenez, J. L.: O/C and OM/OC ratios of
9 primary, secondary, and ambient organic aerosols with high-resolution time-of-flight aerosol
10 mass spectrometry, *Environ. Sci. Technol.*, 42(12), 4478–4485, doi:10.1021/es73009q, 2008.
- 11 Altieri, K. E., Carlton, A. G., Lim, H.-J., Turpin, B. J. and Seitzinger, S. P.: Evidence for
12 oligomer formation in clouds: Reactions of isoprene oxidation products, *Environ. Sci. Technol.*,
13 40(16), 4956–4960, doi:10.1021/es052170n, 2006.
- 14 Altieri, K. E., Seitzinger, S. P., Carlton, A. G., Turpin, B. J., Klein, G. C. and Marshall, A. G.:
15 Oligomers formed through in-cloud methylglyoxal reactions: Chemical composition, properties,
16 and mechanisms investigated by ultra-high resolution FT-ICR mass spectrometry, *Atmos.*
17 *Environ.*, 42(7), 1476–1490, doi:10.1016/j.atmosenv.2007.11.015, 2008.
- 18 Arakaki, T. and Faust, B. C.: Sources, sinks, and mechanisms of hydroxyl radical (\bullet OH)
19 photoproduction and consumption in authentic acidic continental cloud waters from Whiteface
20 Mountain, New York: The role of the Fe (r)(r= II, III) photochemical cycle, *J. Geophys. Res.-*
21 *Atmos.*, (1984–2012), 103(D3), 3487–3504, doi:10.1029/97JD02795, 1998.
- 22 Bethel, H. L., Atkinson, R., and Arey, J.: Hydroxycarbonyl products of the reactions of selected
23 diols with the OH radical, *J. Phys. Chem. A*, 107(32), 6200–6205, doi:10.1021/jp0276931, 2003.
- 24 Canagaratna, M. R., Jayne, J. T., Jimenez, J. L., Allan, J. D., Alfarra, M. R., Zhang, Q., Onasch,
25 T. B., Drewnick, F., Coe, H., Middlebrook, A., Delia, A., Williams, L. R., Trimborn, A. M.,
26 Northway, M. J., DeCarlo, P. F., Kolb, C. E., Davidovits, P. and Worsnop, D. R.: Chemical and
27 microphysical characterization of ambient aerosols with the aerodyne aerosol mass spectrometer,

- 1 Mass. Spectrom. Rev., 26(2), 185–222, doi:10.1002/mas.20115, 2007.
- 2 Carlton, A. G., Turpin, B. J., Altieri, K. E., Seitzinger, S., Reff, A., Lim, H.-J. and Ervens, B.:
3 Atmospheric oxalic acid and SOA production from glyoxal: Results of aqueous photooxidation
4 experiments, Atmos. Environ., 41(35), 7588–7602, doi:10.1016/j.atmosenv.2007.05.035, 2007.
- 5 Daumit, K. E., Kessler, S. H. and Kroll, J. H.: Average chemical properties and potential
6 formation pathways of highly oxidized organic aerosol, Faraday Discuss., 165, 181,
7 doi:10.1039/c3fd00045a, 2013.
- 8 DeCarlo, P. F., Kimmel, J. R., Trimborn, A., Northway, M. J., Jayne, J. T., Aiken, A. C., Gonin,
9 M., Fuhrer, K., Horvath, T., Docherty, K. S., Worsnop, D. R. and Jimenez, J. L.: Field-
10 deployable, high-resolution, time-of-flight aerosol mass spectrometer, Anal. Chem., 78(24),
11 8281–8289, doi:10.1021/ac061249n, 2006.
- 12 Donahue, N. M., Henry, K. M., Mentel, T. F., Kiendler-Scharr, A., Spindler, C., Bohn, B.,
13 Brauers, T., Dorn, H. P., Fuchs, H., Tillmann, R., Wahner, A., Saathoff, H., Naumann, K.-H.,
14 Mohler, O., Leisner, T., Muller, L., Reinnig, M.-C., Hoffmann, T., Salo, K., Hallquist, M., Frosch,
15 M., Bilde, M., Tritscher, T., Barmet, P., Praplan, A. P., DeCarlo, P. F., Dommen, J., Prevot, A. S.
16 H. and Baltensperger, U.: Aging of biogenic secondary organic aerosol via gas-phase OH radical
17 reactions, P. Natl. Acad. Sci., 109(34), 13503–13508, doi:10.1073/pnas.1115186109/-
18 /DCSupplemental, 2012.
- 19 Donahue, N. M., Robinson, A. L., Trump, E. R., Riipinen, I., and Kroll, J. H.: Volatility and
20 aging of atmospheric organic aerosol, Top. Curr. Chem., 339, 97-144,
21 doi:10.1007/128_2012_355, 2014.
- 22 Dzepina, K., Volkamer, R. M., Madronich, S., Tulet, P., Ulbrich, I. M., Zhang, Q., Cappa, C. D.,
23 Ziemann, P. J. and Jimenez, J. L.: Evaluation of recently-proposed secondary organic aerosol
24 models for a case study in Mexico City, Atmos. Chem. Phys., 9(15), 5681–5709,
25 doi:10.5194/acp-0-5681-2009, 2009.
- 26 Dzepina, K., Cappa, C. D., Volkamer, R. M., Madronich, S., DeCarlo, P. F., Zaveri, R. A. and

1 Jimenez, J. L.: Modeling the multiday evolution and aging of secondary organic aerosol during
2 MILAGRO 2006, *Environ. Sci. Technol.*, 45(8), 3496–3503, doi:10.1021/es103186f, 2011.

3 Ervens, B., Turpin, B. J. and Weber, R. J.: Secondary organic aerosol formation in cloud droplets
4 and aqueous particles (aqSOA): a review of laboratory, field and model studies, *Atmos. Chem.
5 Phys.*, 11(21), 11069–11102, doi:10.5194/acp-11-11069-2011, 2011.

6 Ervens, B., Feingold, G., Frost, G. J., and Kreidenweis, S. M.: A modeling study of aqueous
7 production of dicarboxylic acids: 1. Chemical pathways and speciated organic mass production, *J.
8 Geophys. Res.*, 109(D15205), doi:10.1029/2003JD004387, 2004.

9 Faust, B. C. and Hoigne, J.: Photolysis of Fe (III)-hydroxy complexes as sources of OH radicals
10 in clouds, fog and rain, *Atmos. Environ. A.-Gen.*, 24(1), 79–89, doi:10.1016/0960-
11 1686(90)09443-Q, 1990.

12 Galloway, M. M., Chhabra, P. S., Chan, A., Surratt, J. D., Flagan, R. C., Seinfeld, J. H. and
13 Keutsch, F. N.: Glyoxal uptake on ammonium sulphate seed aerosol: reaction products and
14 reversibility of uptake under dark and irradiated conditions, *Atmos. Chem. Phys.*, 9(10), 3331–
15 3345, doi:10.5194/acp-9-3331-2009, 2009.

16 Heald, C. L., Kroll, J. H., Jimenez, J. L., Docherty, K. S., DeCarlo, P. F., Aiken, A. C., Chen, Q.,
17 Martin, S. T., Farmer, D. K. and Artaxo, P.: A simplified description of the evolution of organic
18 aerosol composition in the atmosphere, *Geophys. Res. Lett.*, 37(8), doi:10.1029/2010GL042737,
19 2010.

20 Herrmann, H., Hoffmann, D., Schaefer, T., Brüner, P. and Tilgner, A.: Tropospheric
21 aqueous-phase free-radical chemistry: Radical sources, spectra, reaction kinetics and prediction
22 tools, *Chem. Phys. Chem.*, 11(18), 3796–3822, doi:10.1002/cphc.201000533, 2010.

23 Hodzic, A., Jimenez, J. L., Madronich, S., Canagaratna, M. R., DeCarlo, P. F., Kleinman, L. and
24 Fast, J.: Modeling organic aerosols in a megacity: potential contribution of semi-volatile and
25 intermediate volatility primary organic compounds to secondary organic aerosol formation,
26 *Atmos. Chem. Phys.*, 10(12), 5491–5514, doi:10.5194/acp-10-5491-2010, 2010.

1 Hoffmann, P., Dedik, A. N., Ensling, J., Weinbruch, S., Weber, S., Sinner, T., Gütlich, P. and
2 Ortner, H. M.: Speciation of iron in atmospheric aerosol samples, *J. Aerosol Sci.*, 27(2), 325–337,
3 doi:10.1016/0021-8502(95)00563-3, 1996.

4 Jimenez, J. L., Canagaratna, M. R., Donahue, N. M., Prevot, A., Zhang, Q., Kroll, J. H., DeCarlo,
5 P. F., Allan, J. D., Coe, H. and Ng, N. L.: Evolution of organic aerosols in the atmosphere,
6 *Science*, 326(5959), 1525–1529, doi:10.1126/science.1180353, 2009.

7 Kameel, F. R., Hoffmann, M. R. and Colussi, A. J.: OH Radical-Initiated Chemistry of Isoprene
8 in Aqueous Media. Atmospheric Implications, *J. Phys. Chem. A*, 117(24), 5117–5123,
9 doi:10.1021/jp4026267, 2013.

10 Kirkland, J. R., Lim, Y. B., Tan, Y., Altieri, K. E. and Turpin, B. J.: Glyoxal secondary organic
11 aerosol chemistry: effects of dilute nitrate and ammonium and support for organic radical-radical
12 oligomer formation, *Environ. Chem.*, 10(3), 158–166, doi:10.1071/EN13074, 2013.

13 Kroll, J. H., Smith, J. D., Che, D. L., Kessler, S. H., Worsnop, D. R., and Wilson, K. R.:
14 Measurement of fragmentation and functionalization pathways in the heterogeneous oxidation of
15 oxidized organic aerosol, *Phys. Chem. Chem. Phys.*, 11(36), 8005-8014, doi:10.1039/b905289e,
16 2009.

17 Kroll, J. H., Donahue, N. M., Jimenez, J. L., Kessler, S. H., Canagaratna, M. R., Wilson, K. R.,
18 Altieri, K. E., Mazzoleni, L. R., Wozniak, A. S., Bluhm, H., Mysak, E. R., Smith, J. D., Kolb, C.
19 E. and Worsnop, D. R.: Carbon oxidation state as a metric for describing the chemistry of
20 atmospheric organic aerosol, *Nat. Chem.*, 3(2), 133–139, doi:10.1038/nchem.948, 2011.

21 Lee, A. K., Herckes, P., Leaitch, W. R., Macdonald, A. M. and Abbatt, J.: Aqueous OH oxidation
22 of ambient organic aerosol and cloud water organics: Formation of highly oxidized products,
23 *Geophys. Res. Lett.*, 38(11), doi:10.1029/2011GL047439, 2011a.

24 Lee, A. K., Zhao, R., Gao, S. S. and Abbatt, J.: Aqueous-phase OH oxidation of glyoxal:
25 application of a novel analytical approach employing aerosol mass spectrometry and
26 complementary off-line techniques, *J. Phys. Chem. A*, 115(38), 10517–10526,

1 doi:10.1021/jp20204099g, 2011b.

2 Lee, A. K., Hayden, K. L., Herckes, P., Leaitch, W. R., Liggio, J., Macdonald, A. M. and Abbatt,
3 J.: Characterization of aerosol and cloud water at a mountain site during WACS 2010: secondary
4 organic aerosol formation through oxidative cloud processing, *Atmos. Chem. Phys.*, 12(15),
5 7103–7116, doi:10.5194/acp-12-7103-2012, 2012.

6 Lee-Taylor, J., Madronich, S., Aumont, B., Baker, A., Camredon, M., Hodzic, A., Tyndall, G. S.,
7 Apel, E. and Zaveri, R. A.: Explicit modeling of organic chemistry and secondary organic aerosol
8 partitioning for Mexico City and its outflow plume, *Atmos. Chem. Phys.*, 11(24), 13219–13241,
9 doi:10.5194/acp-11-13219-2011, 2011.

10 Lim, Y. B., Tan, Y., Perri, M. J., Seitzinger, S. P. and Turpin, B. J.: Aqueous chemistry and its
11 role in secondary organic aerosol (SOA) formation, *Atmos. Chem. Phys.*, 10(21), 10521–10539,
12 doi:10.5194/acp-10-10521-2010, 2010.

13 Liu, Y., Monod, A., Tritscher, T., Praplan, A. P., DeCarlo, P. F., Temime-Roussel, B., Quivet, E.,
14 Marchand, N., Dommen, J. and Baltensperger, U.: Aqueous phase processing of secondary
15 organic aerosol from isoprene photooxidation, *Atmos. Chem. Phys.*, 12(13), 5879–5895,
16 doi:10.5194/acp-12-5879-2012, 2012a.

17 Liu, Y., Siekmann, F., Renard, P., Zein, El, A., Salque, G., Haddad, El, I., Temime-Roussel, B.,
18 Voisin, D., Thissen, R. and Monod, A.: Oligomer and SOA formation through aqueous phase
19 photooxidation of methacrolein and methyl vinyl ketone, *Atmos. Environ.*, 49, 123–129,
20 doi:10.1016/j.atmosenv.2011.12.012, 2012b.

21 Ma, J., Ma, W., Song, W., Chen, C., Tang, Y., Huang, Y., Xu, Y., Zang, L. and Zhao, J.: Fenton
22 degradation of organic pollutants in the presence of low-molecular-weight organic acids:
23 Cooperative effect of quinone and visible light, *Environ. Sci. Technol.*, 40(2), 618–624,
24 doi:10.1021/es051657t, 2006.

25 Mensah, A. A., Buchholz, A., Mentel, Th. F., Tillmann, R., Kiendler-Scharr, A.: Aerosol mass
26 spectrometric measurements of stable crystal hydrates of oxalates and inferred relative ionization

1 efficiency of water, *J. Aerosol Sci.*, 42(1), 11-19, doi:10.1016/j.jaerosci.2010.10.003, 2011.

2 Nguyen, T. B., Coggon, M. M., Flagan, R. C. and Seinfeld, J. H.: Reactive Uptake and Photo-
3 Fenton Oxidation of Glycolaldehyde in Aerosol Liquid Water, *Environ. Sci. Technol.*, 47(9),
4 4307–4316, doi:10.1021/es400538j, 2013.

5 Nozière, B., Dziedzic, P. and Córdova, A.: Products and Kinetics of the Liquid-Phase Reaction of
6 Glyoxal Catalyzed by Ammonium Ions (NH_4^+), *J. Phys. Chem. A*, 113(1), 231–237,
7 doi:10.1021/jp8078293, 2009.

8 Ortiz-Montalvo, D. L., Lim, Y. B., Perri, M. J., Seitzinger, S. P. and Turpin, B. J.: Volatility and
9 yield of glycolaldehyde SOA formed through aqueous photochemistry and droplet evaporation,
10 *Aerosol Sci. Tech.*, 46(9), 1002–1014, doi:10.1080/02786826.2012.686676, 2012.

11 Ou, X., Quan, X., Chen, S., Zhang, F. and Zhao, Y.: Photocatalytic reaction by Fe (III)–citrate
12 complex and its effect on the photodegradation of atrazine in aqueous solution, *J. Photoch.*
13 *Photobio. A*, 197(2-3), 382–388, doi:10.1016/j.jphotochem.2008.02.001, 2008.

14 Perri, M. J., Seitzinger, S. and Turpin, B. J.: Secondary organic aerosol production from aqueous
15 photooxidation of glycolaldehyde: Laboratory experiments, *Atmos. Environ.*, 43(8), 1487–1497,
16 doi:10.1016/j.atmosenv.2008.11.037, 2009.

17 Perri, M. J., Lim, Y. B., Seitzinger, S. P. and Turpin, B. J.: Organosulfates from glycolaldehyde
18 in aqueous aerosols and clouds: Laboratory studies, *Atmos. Environ.*, 44(21), 2658–2664,
19 doi:10.1016/j.atmosenv.2010.03.031, 2010.

20 Presto, A. A. and Donahue, N. M.: Investigation of α -pinene+ ozone secondary organic aerosol
21 formation at low total aerosol mass, *Environ. Sci. Technol.*, 40(11), 3536–3543,
22 doi:10.1021/es052203z, 2006.

23 Qi, L., Nakao, S., Malloy, Q., Warren, B. and Cocker, D. R., III: Can secondary organic aerosol
24 formed in an atmospheric simulation chamber continuously age?, *Atmos. Environ.*, 44(25), 2990–
25 2996, doi:10.1016/j.atmosenv.2010.05.020, 2010.

1 Renard, P., Siekmann, F., Gandolfo, A., Socorro, J., Salque, G., Ravier, S., Quivet, E., Clément, J.
2 L., Traikia, M., Delort, A. M., Voisin, D., Vuitton, V., Thissen, R. and Monod, A.: Radical
3 mechanisms of methyl vinyl ketone oligomerization through aqueous phase OH-oxidation: on the
4 paradoxical role of dissolved molecular oxygen, *Atmos. Chem. Phys.*, 13(13), 6473–6491,
5 doi:10.5194/acp-13-6473-2013, 2013.

6 Sander, R.: Compilation of Henry's law constants for inorganic and organic species of potential
7 importance in environmental chemistry, (Version 3), <http://www.henrys-law.org>, 1999.

8 Seinfeld, J. H., and Pandis, S. N.: *Atmospheric Chemistry and Physics: From Air Pollution to*
9 *Climate Change*, 2nd Edition, John Wiley & Sons, Inc., Hoboken, New Jersey, 2006.

10 Smith, J., Sio, V., Yu, L., Zhang, Q. and Anastasio, C.: Secondary Organic Aerosol Production
11 from Aqueous Reactions of Atmospheric Phenols with an Organic Triplet Excited State, *Environ.*
12 *Sci. Technol.*, 48(2), 1049–1057, doi:10.1021/es4045715, 2014.

13 Sorooshian, A., Wang, Z., Coggon, M. M., Jonsson, H. H. and Ervens, B.: Observations of Sharp
14 Oxalate Reductions in Stratocumulus Clouds at Variable Altitudes: Organic Acid and Metal
15 Measurements During the 2011 E-PEACE Campaign, *Environ. Sci. Technol.*, 47(14), 7747–7756,
16 doi:10.1021/es4012383, 2013.

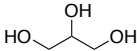
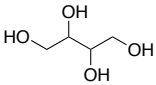
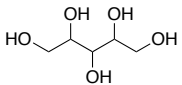
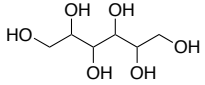
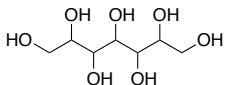
17 Southworth, B. A. and Voelker, B. M.: Hydroxyl radical production via the photo-Fenton
18 reaction in the presence of fulvic acid, *Environ. Sci. Technol.*, 37(6), 1130–1136,
19 doi:10.1021/es0207571, 2003.

20 Sun, Y. L., Zhang, Q., Anastasio, C. and Sun, J.: Insights into secondary organic aerosol formed
21 via aqueous-phase reactions of phenolic compounds based on high resolution mass spectrometry,
22 *Atmos. Chem. Phys.*, 10(10), 4809–4822, doi:10.5194/acp-10-4809-2010, 2010.

23 Takegawa, N., Miyakawa, T., Kawamura, K. and Kondo, Y.: Contribution of selected
24 dicarboxylic and ω -oxocarboxylic acids in ambient aerosol to the m/z 44 signal of an Aerodyne
25 aerosol mass spectrometer, *Aerosol Sci. Tech.*, 41(4), 418–437,
26 doi:10.1080/02786820701203215, 2007.

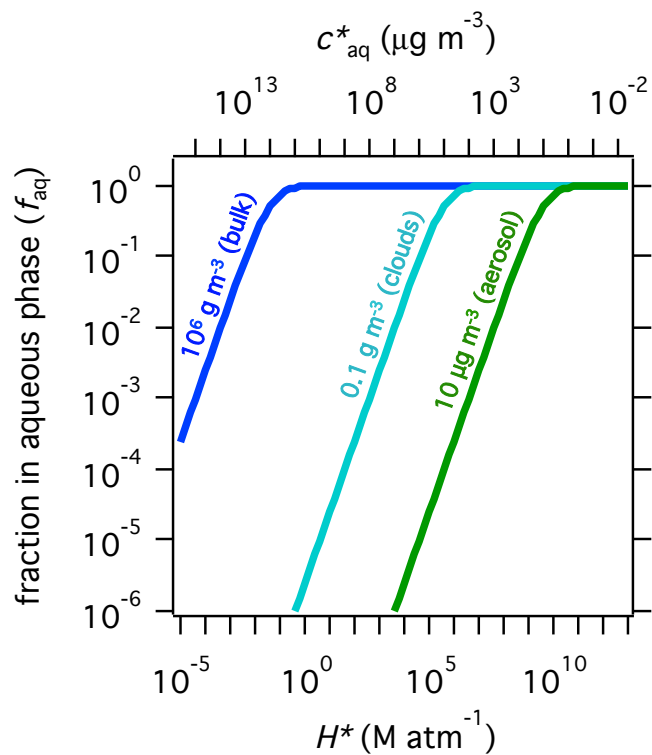
- 1 Tan, Y., Perri, M. J., Seitzinger, S. P. and Turpin, B. J.: Effects of Precursor Concentration and
2 Acidic Sulfate in Aqueous Glyoxal– OH Radical Oxidation and Implications for Secondary
3 Organic Aerosol, *Environ. Sci. Technol.*, 43(21), 8105–8112, doi:10.1021/es901742f, 2009.
- 4 Tan, Y., Carlton, A. G., Seitzinger, S. P. and Turpin, B. J.: SOA from methylglyoxal in clouds
5 and wet aerosols: Measurement and prediction of key products, *Atmos. Environ.*, 44(39), 5218–
6 5226, doi:10.1016/j.atmosenv.2010.08.045, 2010.
- 7 Tilgner, A. and Herrmann, H.: Radical-driven carbonyl-to-acid conversion and acid degradation
8 in tropospheric aqueous systems studied by CAPRAM, *Atmos. Environ.*, 44(40), 5415–5422,
9 doi:10.1016/j.atmosenv.2010.07.050, 2010.
- 10 Volkamer, R., Jimenez, J. L., San Martini, F., Dzepina, K., Zhang, Q., Salcedo, D., Molina, L. T.,
11 Worsnop, D. R. and Molina, M. J.: Secondary organic aerosol formation from anthropogenic air
12 pollution: Rapid and higher than expected, *Geophys. Res. Lett.*, 33(17),
13 doi:10.1029/2006GL026899, 2006.
- 14 Volkamer, R., Ziemann, P. J. and Molina, M. J.: Secondary organic aerosol formation from
15 acetylene (C₂H₂): Seed effect on SOA yields due to organic photochemistry in the aerosol
16 aqueous phase, *Atmos. Chem. Phys.*, 9(6), 1907–1928, doi:10.5194/acp-9-1907-2009, 2009.
- 17 Zhang, X., Chen, Z. M. and Zhao, Y.: Laboratory simulation for the aqueous OH-oxidation of
18 methyl vinyl ketone and methacrolein: significance to the in-cloud SOA production, *Atmos.*
19 *Chem. Phys.*, 10(19), 9551–9561, doi:10.5194/acp-10-9551-2010, 2010.
- 20 Zhao, R., Lee, A. and Abbatt, J.: Investigation of aqueous-phase photooxidation of glyoxal and
21 methylglyoxal by aerosol chemical ionization mass spectrometry: observation of
22 hydroxyhydroperoxide formation, *J. Phys. Chem. A*, 116(24), 6253–6263,
23 doi:10.1021/jp211528d, 2012.
- 24 Zuo, Y. and Hoigne, J.: Formation of hydrogen peroxide and depletion of oxalic acid in
25 atmospheric water by photolysis of iron (III)-oxalato complexes, *Environ. Sci. Technol.*, 26(5),
26 1014–1022, doi:10.1021/es00029a022, 1992.

1 Table 1. Initial concentrations of reactants in the atomizer solutions.

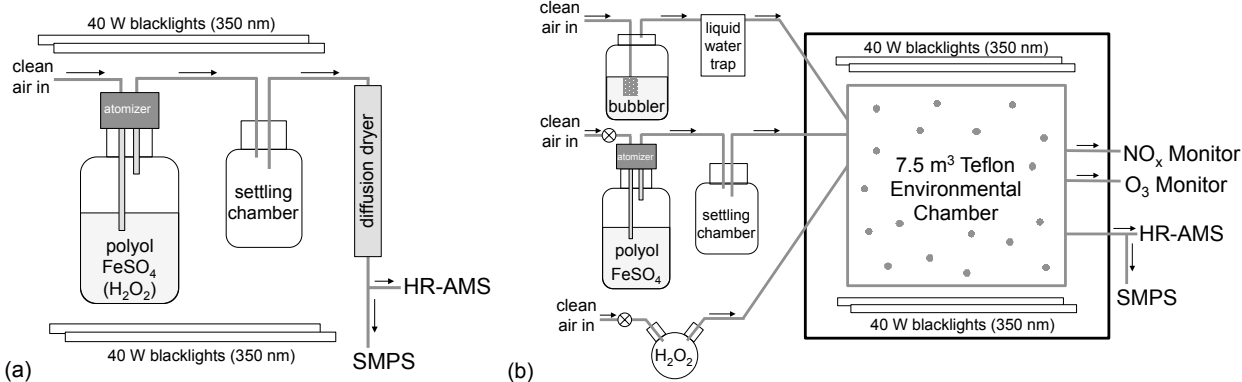
Polyol Precursor		Bulk Experiments			Chamber Experiments		
Name & Formula	Chemical Structure	[Polyol] (mM)	[FeSO ₄] (mM)	[H ₂ O ₂] (mM)	[Polyol] ^a (mM)	[FeSO ₄] ^a (mM)	[H ₂ O ₂] ^b (mM)
Glycerol (C ₃ H ₈ O ₃)		0.20	0.45	2.0	2.0	0.40	27
Erythritol (C ₄ H ₁₀ O ₄)		0.20	0.42	2.0	2.0	0.39	27
Adonitol (C ₅ H ₁₂ O ₅)		0.20	0.41	2.0	2.0	0.40	27
Mannitol (C ₆ H ₁₄ O ₆)		0.22	0.42	2.0	2.0	0.38	27
Volemitol (C ₇ H ₁₆ O ₇)		0.19	0.40	2.0	2.0	0.40	27

2 ^a Initial concentrations in the atomizer solution; the aqueous particles themselves will be
 3 substantially more concentrated (by a factor of ~1000).

4 ^b Estimated concentrations within the particles, calculated by assuming full evaporation of H₂O₂
 5 into the chamber, with Henry's Law partitioning into the aqueous particles; likely represent an
 6 upper limit.

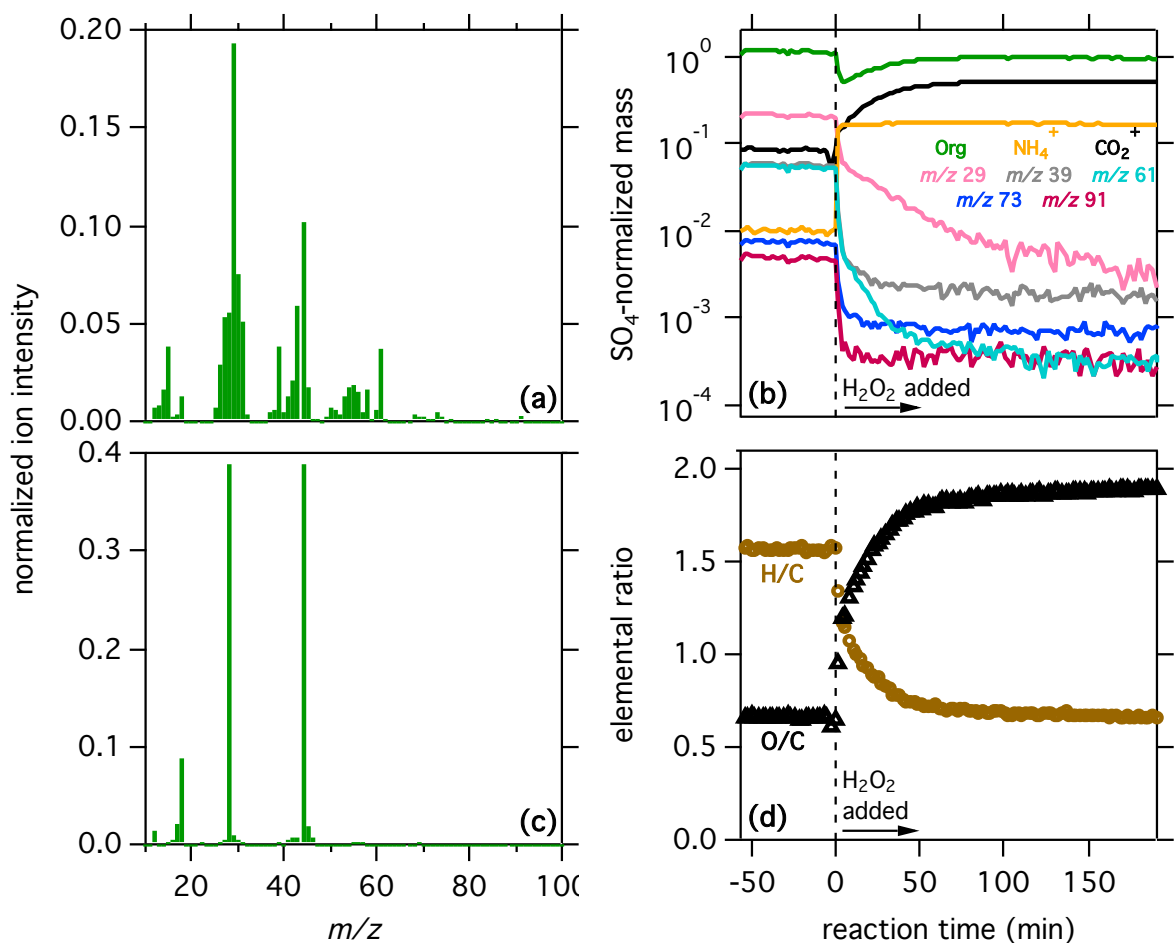


1
 2 Figure 1. The fraction of a compound that will partition to the aqueous phase (f_{aq}) as a function of
 3 its Henry's Law constant, H^* (or alternatively its saturation vapor concentration, c^*_{aq}), and the
 4 liquid water content (LWC). Compounds with $0.1 \text{ M atm}^{-1} < H^* < 10^9 \text{ M atm}^{-1}$ will be primarily
 5 in the aqueous phase at bulk LWC (blue line), but primarily in the gas phase at aqueous aerosol
 6 LWC (green line). Cloud water (teal line) represents the intermediate case, with more partitioning
 7 into the aqueous phase than for aqueous particles, but still with far less than for a bulk aqueous
 8 solution.

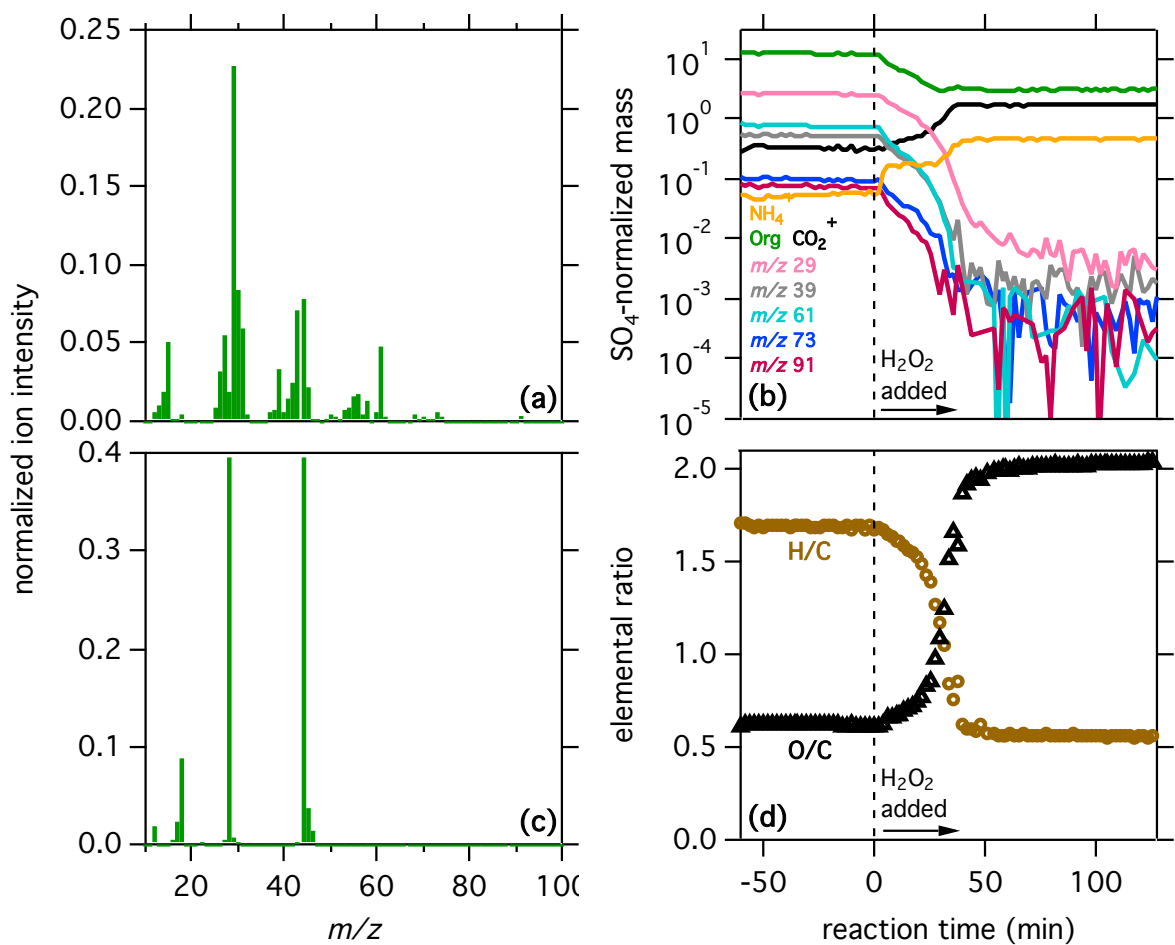


1 (a) (b)

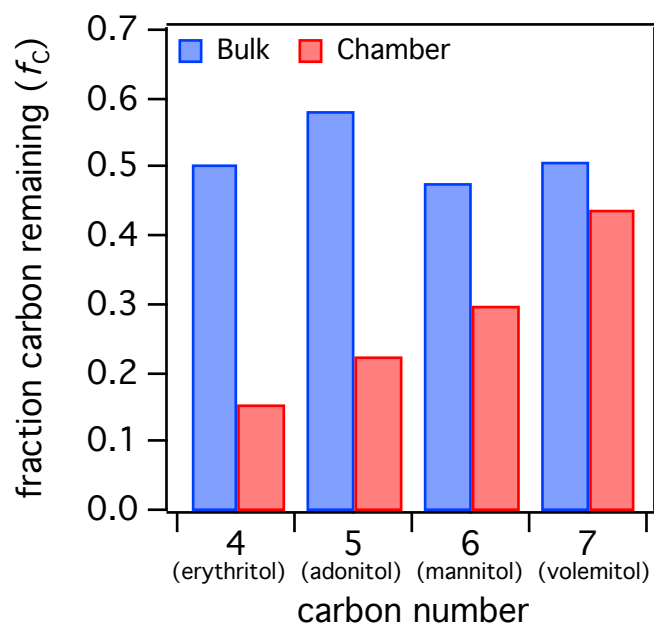
2 Figure 2. Experimental set-up for (a) bulk experiments and (b) chamber experiments. The
 3 atomizer serves as a reactor for bulk oxidation but only as a source of aqueous particles for
 4 chamber oxidation. In the bulk experiments, the solution is continuously atomized, with H_2O_2
 5 added after the polyol and FeSO_4 have been sampled for 1 hour. In the chamber experiments, a
 6 solution containing the polyol and FeSO_4 is atomized into the chamber for 1 hour, with gas-phase
 7 H_2O_2 introduced later via the two-neck flask. Humidified make-up air is continuously supplied to
 8 the chamber via the bubbler. While the focus of this work is dark Fenton chemistry, UV lights are
 9 turned on following oxidation in both set-ups in order to assess the photo-reactivity of the
 10 reaction products.



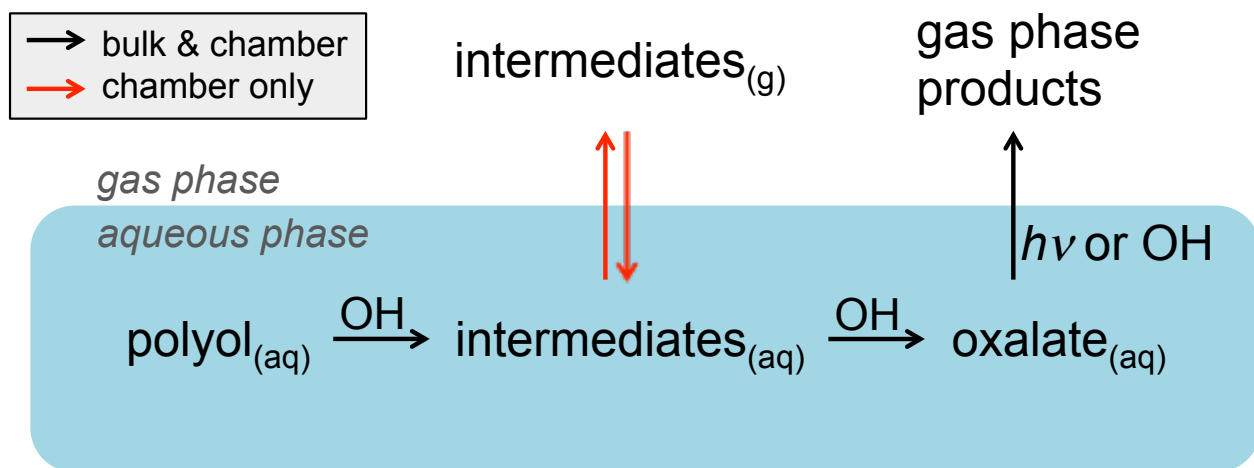
1
 2 Figure 3. Results for the oxidation of erythritol within the bulk aqueous phase: (a) AMS spectra
 3 of unreacted erythritol; (b) sulfate-normalized mass concentrations of total organic (Org),
 4 ammonium (NH₄⁺), CO₂⁺, and key ions associated with erythritol (*m/z* 29, 39, 61, 73, 91) as a
 5 function of reaction time; (c) AMS spectra of oxidation products; and (d) oxygen-to-carbon and
 6 hydrogen-to-carbon ratios as a function of reaction time. Results in panels a, c, and d are from
 7 high-resolution mass spectrometric analysis. All traces in panel b are from unit mass resolution,
 8 except NH₄⁺ and CO₂⁺, which are high-resolution traces.



1
 2 Figure 4. Same as Figure 3, but for the oxidation of erythritol within submicron particles
 3 (chamber experiments): (a) AMS spectra of unreacted erythritol; (b) sulfate-normalized mass
 4 concentrations of total organic (Org), ammonium (NH_4^+), CO_2^+ , and key ions associated with
 5 erythritol (m/z 29, 39, 61, 73, 91) as a function of reaction time; (c) AMS spectra of oxidation
 6 products; and (d) oxygen-to-carbon and hydrogen-to-carbon ratios as a function of reaction time.



1
 2 Figure 5. The fraction of carbon remaining in the condensed phase after oxidation (f_c) in the bulk
 3 solution (blue bars) or in submicron particles (red bars), as calculated from Eq. 2, using high-
 4 resolution V mode data. Meaningful values could not be determined for the oxidation of glycerol
 5 (C3) due to evaporation from the particle phase prior to oxidation.



1

2 Figure 6. Simplified mechanism to explain observed differences between oxidation in the bulk

3 and in submicron particles. The polyol reacts to form intermediates with lower H^* (higher

4 volatility over water), which remain fully in the aqueous phase during bulk experiments, but

5 partition to the gas phase (red arrows) during chamber experiments. This partitioning, which

6 occurs to a greater extent for smaller polyol precursors, competes with further aqueous oxidation,

7 and has the effect of lowering the product (oxalate) yield. Upon exposure to ultraviolet light, the

8 Fe(III) oxalato complex photolyzes, forming small gas-phase products.

9

10